

## Effect of Nd<sub>2</sub>O<sub>3</sub> Particles Addition on the Crack Resistance of Micro-arc Oxidation Coatings on Cast Aluminum Alloy

Ping Wang<sup>1,2,3</sup>, Xiao Wei Wei<sup>1,\*</sup>, Jun Pu<sup>2</sup>, Dan Xiong<sup>2</sup>, Ji Wei Liu<sup>2</sup>, Ze Yu Gong<sup>2</sup>, Jie Hu<sup>2</sup>,  
Wen Jie Cao<sup>2</sup>, Xiao Tao Zu<sup>3,\*</sup>

<sup>1</sup> The Postdoctoral Station at Xihua University Based on Collaboration Innovation Center of Sichuan Automotive Key Parts, School of Materials Science and Engineering, Xihua University, Chengdu, 610039, China

<sup>2</sup> School of Materials Science and Engineering, Southwest Petroleum University, Chengdu, 610500, China

<sup>3</sup> School of Physics, University of Electronic Science and Technology of China, Chengdu, 611731, China

\*E-mail: [weixiaowei90@yeah.net](mailto:weixiaowei90@yeah.net)

Received: 17 February 2019 / Accepted: 9 April 2019 / Published: 10 May 2019

---

Micro-arc oxidation coatings were fabricated on cast aluminum alloy in electrolytes with the Nd<sub>2</sub>O<sub>3</sub> particles addition varying from 0 to 0.4 g/L. The microstructure, phase composition, corrosion resistance and thermal shock resistance of the coatings were characterized by Scanning Electron Microscopy (SEM), X-ray Diffraction (XRD), Electrochemical Workstation and Chamber Electric Furnace, respectively. It was found that the size of the micropores on the surface of the coatings increased with the addition of the Nd<sub>2</sub>O<sub>3</sub> particles, while the number of micropores gradually decreased. After the thermal shock tests, the holes on the coating surface decreased, and the coatings became more compact with the addition of the Nd<sub>2</sub>O<sub>3</sub> particles; furthermore, the cracks also decreased and even disappeared with an increase in the Nd<sub>2</sub>O<sub>3</sub> particle concentration, which proved that adding Nd<sub>2</sub>O<sub>3</sub> particles in the electrolytes could substantially strengthen the thermal shock resistance of the coatings. The results of the XRD analyses indicated that the coatings mainly consisted of  $\gamma$ -Al<sub>2</sub>O<sub>3</sub>, SiO<sub>2</sub> and Si phases. In addition, the corrosion rate of the coatings decreased slightly with the addition of the Nd<sub>2</sub>O<sub>3</sub> particles; thus the corrosion resistance of the coatings was gradually improved.

---

**Keywords:** Micro-arc oxidation; Cast aluminum alloy; Nd<sub>2</sub>O<sub>3</sub> particles; Crack resistance

### 1. INTRODUCTION

Cast aluminum alloys are widely used in automobile engine pistons due to their excellent properties, such as high specific strength, low density and easy processability [1-2]. However, low thermal strength and poor high-temperature mechanical properties of cast aluminum alloys limit their

extensive applications [3-5]. Micro-arc oxidation (MAO) technology was developed from anodic oxidation and is widely used on the surfaces of valve metals, such as aluminum, magnesium, titanium and their alloys, and is considered to be one of the most economical and environmentally friendly surface modification technologies [6-7]. The thermal expansion properties of the MAO coatings are inconsistent with the matrix material, which may cause microcracks on the coating surface, and then the stress may expand and even the coating peeling phenomenon occurs, resulting in the failure of the thermal barrier and corrosion resistance of the coating[8-9]. Thus, it is imperative to change the thermal expansion properties and increase the adhesive strength of the coating. In recent years, domestic and overseas attention had been paid to the influence of doped particles in the electrolytes on the micro-arc oxidation coatings. The doping of particles in electrolytes, such as  $\text{Al}_2\text{O}_3$  [10],  $\text{MgO}$  [11], and  $\text{TiO}_2$  [12], has been widely studied. Neodymium oxide ( $\text{Nd}_2\text{O}_3$ ) is an inorganic chemical product. It has been reported that  $\text{Nd}_2\text{O}_3$  can be used as a blending agent for high-temperature ceramics in the ceramic industry [13]. However, there is no research on doping  $\text{Nd}_2\text{O}_3$  particles into electrolytes to improve the comprehensive performance of the MAO coating.

In this paper, MAO coatings were produced on cast aluminum alloy with different  $\text{Nd}_2\text{O}_3$  concentrations in a silicate and phosphate mixed electrolyte system. The voltage-time curves were recorded during the MAO experiment, and the effect of the  $\text{Nd}_2\text{O}_3$  concentration on the microstructure, phase composition, corrosion resistance, coating adhesive strength and thermal shock resistance of the MAO coatings was investigated.

## 2. EXPERIMENTAL

### 2.1. Preparation of MAO coating

In the experiment, parallel hexahedral samples of ZL108 cast aluminum alloy were used as substrate materials. The chemical composition (mass fraction) of ZL108 aluminum alloy is 11.0%-13.0% Si, 1.0%-2.0% Cu, 0.4%-1.0% Mg, 0.3%-0.9% Mn,  $\leq 0.7\%$  Fe,  $\leq 0.3\%$  Ni,  $\leq 0.2\%$  Zn,  $\leq 0.2\%$  Ti,  $\leq 0.05\%$  Pb,  $\leq 0.01\%$  Sn and Al balance. The specimens, with dimensions of  $20 \times 10 \times 3$  mm, were polished and degreased before the experiment. The base electrolyte contained 18 g/L  $\text{Na}_3\text{PO}_4$ , 4 g/L  $\text{Na}_2\text{SiO}_3$ , 0.5 g/L NaOH and 3 mL/L  $\text{C}_3\text{H}_8\text{O}_3$ . The concentrations of the  $\text{Nd}_2\text{O}_3$  particles in the base electrolyte were 0 g/L, 0.1 g/L, 0.2 g/L, 0.3 g/L, and 0.4 g/L. Furthermore, the  $\text{Nd}_2\text{O}_3$  particles were stirred continuously during each experiment in order to maintain uniform dispersal in the electrolyte. The MAO coatings were produced under a peak current density of  $5 \text{ A/dm}^2$  for 30 min, a duty cycle of 50% and a fixed frequency of 100 Hz. The temperature of the electrolyte was kept below  $25^\circ\text{C}$  by a circulatory cooling system during the MAO process. After the MAO process, the samples were rinsed with hot water at  $95^\circ\text{C}$  for 10 min and then dried in warm air.

### 2.2. Coating analysis

The Scanning Electron Microscope (SEM, ZEISS EVO MA15) equipped with an Energy Dispersive Spectrometer (EDS, OXFORD 20) was used to observe the surface and cross-sectional

morphologies of MAO coatings. Phase composition of the coatings was investigated by X-ray Diffraction (XRD, DX-2700B). The diffraction data were acquired over scattering angles  $2\theta$  from  $10^\circ$  to  $80^\circ$  with a scanning speed of  $0.1^\circ \text{ s}^{-1}$ . Scratch tests, which could evaluate the adhesion between the coating and the substrate, were executed by using a multifunctional surface performance tester (MFT-4000) with automatic loading from 0-20 N at a loading rate of 10 N/min. In addition, chamber electric furnace (SX-10-12) was used to evaluate the thermal shock resistance of the coatings, which was heated to  $500^\circ\text{C}$  for 10 min and then cooled down in  $25^\circ\text{C}$  water for 50 cycles. The surface hardness and thickness were investigated by Digital microhardness tester (HXD-2000TM/LCD) at 2 N for 15 s and Digital Thickness Gauges (TT230), respectively. To evaluate the corrosion resistance of MAO coatings, potentiodynamic polarization was applied to acquire corrosion potential, current and corrosion rate in 3.5% NaCl solution at room temperature by Electrochemical Workstation (PGSTAT302N, Switzerland). The polarization curve scanning rate was  $1.5 \text{ mV}\cdot\text{s}^{-1}$  with a potential range from -1.0 V to -0.4 V.

### 3. RESULTS AND DISCUSSION

#### 3.1 Growth process of the coatings

The time-transient behaviors of the voltage response of the MAO coatings with different  $\text{Nd}_2\text{O}_3$  particle concentrations are presented in Fig. 1. All voltage-time curves for the five different specimens showed a rapid increase in voltage at the early MAO stage due to the breakdown of the thin insulating barrier oxidation coating on the Al alloy substrate.

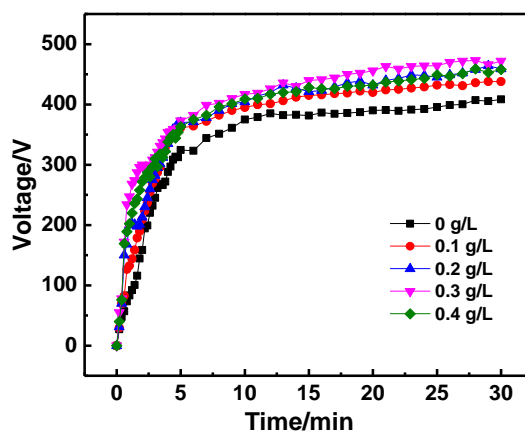


**Figure 1.** Voltage-time curves of the MAO coatings prepared with different concentrations of  $\text{Nd}_2\text{O}_3$  particles.

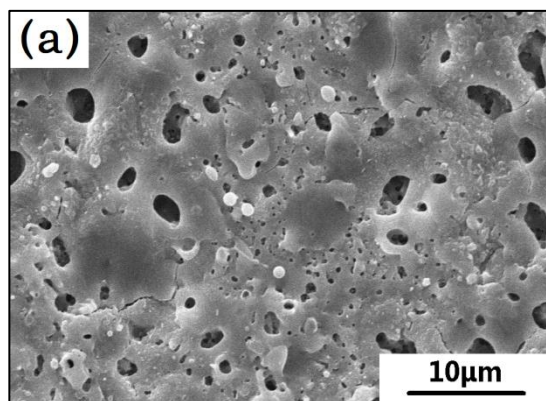
After 5 min, the oxidation voltage became gradually steady along with a very minor rise, indicating that micro-arc oxidation stage came up. It can be seen that by adding  $\text{Nd}_2\text{O}_3$  particles, the voltage value had a distinct increase compared to coatings prepared without  $\text{Nd}_2\text{O}_3$  particles. In addition, the oxidation voltage increased gradually with the addition of  $\text{Nd}_2\text{O}_3$  particles from 0 to 0.3

g/L. The surface charge of the  $\text{Nd}_2\text{O}_3$  particles in electrolytes was  $-15.7$  mV [14] and easily moved towards the anode due to the effects of the electric field and mechanical stirring. With the continued addition of  $\text{Nd}_2\text{O}_3$  particles, the absorption of the  $\text{Nd}_2\text{O}_3$  particles on the surface of the anode strengthened the electrical resistance, which led to the increase in the voltage. At the particle concentration of  $0.4$  g/L, the voltage decreased, which indicated that an excessive particle concentration was detrimental to the growth of the coatings.

### 3.2 The morphologies analysis

#### 3.2.1 Surface morphologies and element content of coatings

Fig. 2 depicts the surface morphologies and the EDS results of the MAO coatings prepared with the different  $\text{Nd}_2\text{O}_3$  particle concentrations. All the MAO coatings exhibited porous microstructures, and it can be observed that there were many micropores on the coating prepared without  $\text{Nd}_2\text{O}_3$  particles (Fig. 2(a)), while the number of micropores on the coating surface decreased gradually and the size of the micropores increased with the addition of the  $\text{Nd}_2\text{O}_3$  particles, as shown in Fig. 2(b)-(e). In addition, the surface of the coatings gradually became uneven, resulting in an increase in the surface roughness. The surface of the MAO coatings exhibited many sintered discs, which were discharge channels formed by the rapid cooling of the coating during the MAO treatment and the number of sintered discs increased with the increment of  $\text{Nd}_2\text{O}_3$  particles concentration. This result indicated that a higher oxidation voltage causes stronger discharge, forming larger discharge channels and more sintered discs. Table 1 shows the EDS results of the coatings prepared with different  $\text{Nd}_2\text{O}_3$  concentrations. Obviously, the Nd content increased with increasing  $\text{Nd}_2\text{O}_3$  concentrations, while the O and Si contents gradually decreased and then increased at the highest  $\text{Nd}_2\text{O}_3$  concentration of  $0.4$  g/L. Due to the addition of  $\text{Nd}_2\text{O}_3$  particles into the electrolytes,  $\text{Nd}_2\text{O}_3$  particles were involved in the formation of the MAO coatings, which influenced the reaction between the electric arcs and the substrate, resulting in changes in element composition of the coatings.



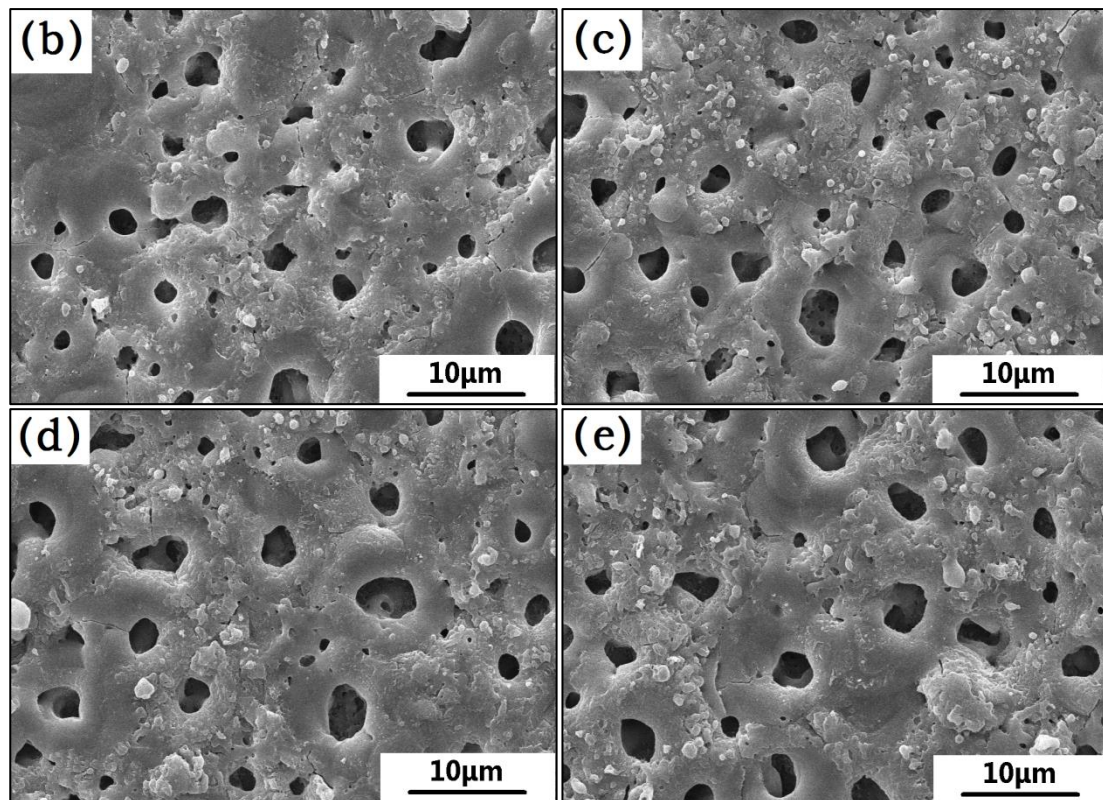


**Figure 2.** Surface morphologies of the MAO coatings prepared with different concentrations of  $\text{Nd}_2\text{O}_3$  particles: (a) 0 g/L, (b) 0.1 g/L, (c) 0.2 g/L, (d) 0.3 g/L, (e) 0.4 g/L.

**Table 1.** EDS results of MAO coatings prepared with different  $\text{Nd}_2\text{O}_3$  concentrations

Atomic %	0 g/L	0.1 g/L	0.2 g/L	0.3 g/L	0.4 g/L
Nd	/	0.20	0.44	1.60	1.95
Al	47.91	52.44	55.22	56.24	53.88
O	41.78	40.64	37.67	37.24	38.94
Si	10.31	6.72	6.67	4.92	5.23

### 3.2.2 Cross-sectional morphologies of the coatings

Fig. 3 shows the cross-sectional microstructures of MAO coatings prepared with different concentrations of  $\text{Nd}_2\text{O}_3$  particles. It can be seen that the thickness of the coatings initially increased and then decreased at the highest  $\text{Nd}_2\text{O}_3$  concentration of 0.4 g/L, which was consistent with the variation of voltage. With the addition of  $\text{Nd}_2\text{O}_3$  particles (0-0.3 g/L), the voltage increased gradually, which led to the increment of discharge intensity and the growth rate of the coatings became faster. At the concentration of 0.4 g/L, the breakdown of the coatings became more difficult due to the thickened coatings and the reduction of the voltage. Thus the coating growth rate slowed down and the thickness of coating decreased at 0.4 g/L  $\text{Nd}_2\text{O}_3$  particles concentration. Furthermore, it can be observed that the coatings with  $\text{Nd}_2\text{O}_3$  particles addition (Fig. 3(b)-(e)) were more tightly bonded with the substrates and were more compact and smooth compared to the coatings prepared without  $\text{Nd}_2\text{O}_3$  particles (Fig. 3(a)),

which attested that the addition of  $\text{Nd}_2\text{O}_3$  particles in the electrolytes could improve the surface quality of the coatings and was also beneficial to the bonding between the coatings and the substrates.

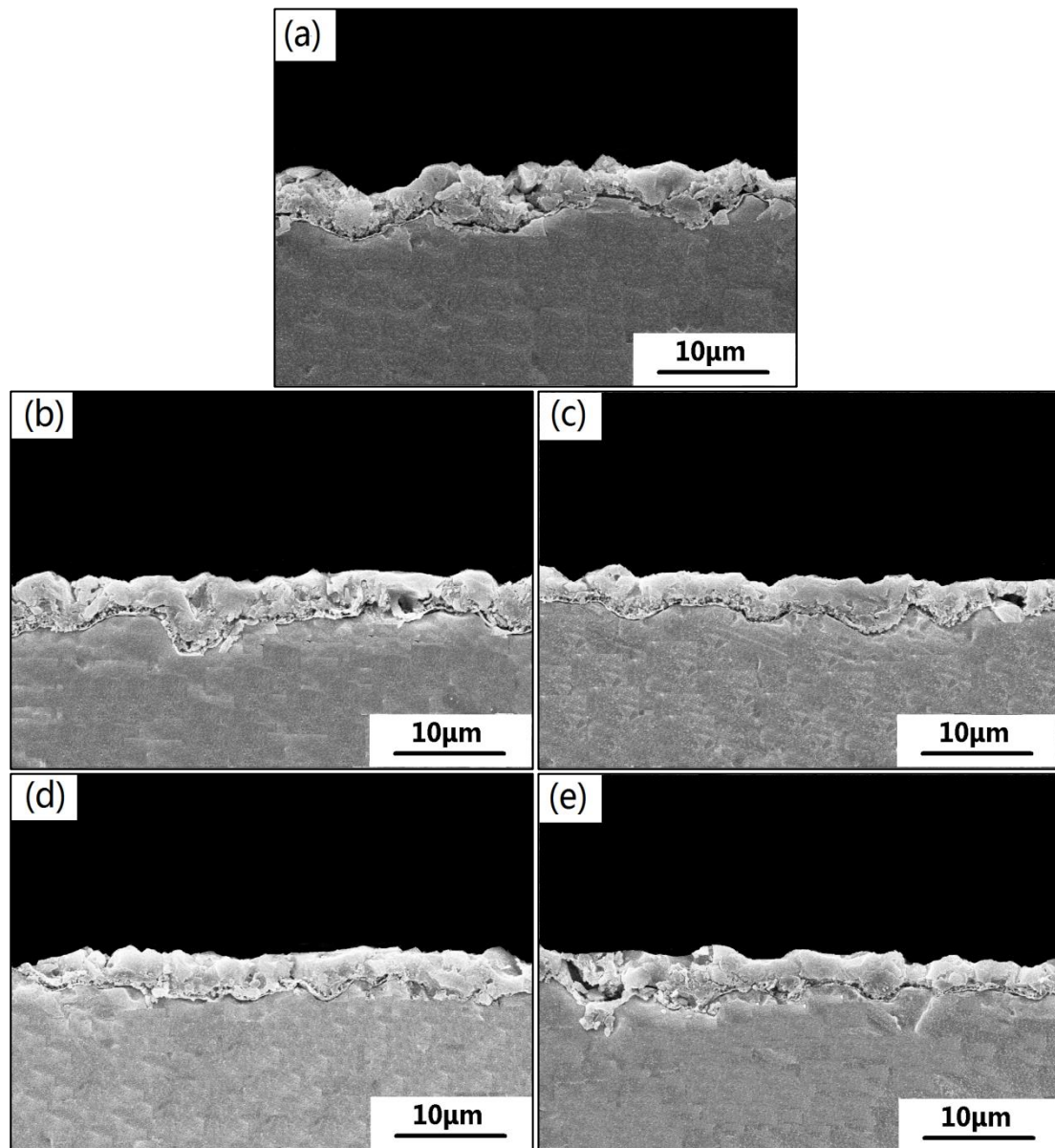


**Figure 3.** Cross-sectional images of the MAO coatings prepared with different  $\text{Nd}_2\text{O}_3$  concentrations: (a) 0 g/L, (b) 0.1 g/L, (c) 0.2 g/L, (d) 0.3 g/L and (e) 0.4 g/L.

### 3.3 The phase composition analysis

Fig. 4 shows the XRD spectra of the MAO coatings prepared using different  $\text{Nd}_2\text{O}_3$  concentrations. It was found that the coatings mainly consisted of  $\gamma\text{-Al}_2\text{O}_3$ ,  $\text{SiO}_2$  and Si phase. There was no apparent signal of  $\text{Nd}_2\text{O}_3$  phase owing to the low  $\text{Nd}_2\text{O}_3$  content. The peak of Al coming from the substrate was detected because the coatings were very thin and X-rays can penetrate into the substrate through the MAO coatings [15]. As shown in equation (4)-(5), the peak of  $\text{SiO}_2$  may come

from the oxidation of Si in the substrate and the disintegration of  $\text{SiO}_3^{2-}$  in the electrolytes. Due to the local high temperature in the MAO process, the amorphous  $\text{Al}_2\text{O}_3$  would gradually transform to  $\gamma\text{-Al}_2\text{O}_3$  [10], as shown in equation (6). The intensity patterns of  $\gamma\text{-Al}_2\text{O}_3$  and  $\text{SiO}_2$  initially increased and then slowly decreased, in accordance with the oxidation voltage. The increased oxidation voltage caused an increase of the micro-arc discharge temperature, which increased the phase transformation efficiency from amorphous  $\text{Al}_2\text{O}_3$  to  $\gamma\text{-Al}_2\text{O}_3$ , and the oxidation of Si and the disintegration of  $\text{SiO}_3^{2-}$  also got faster. The possible reactions are as follows:

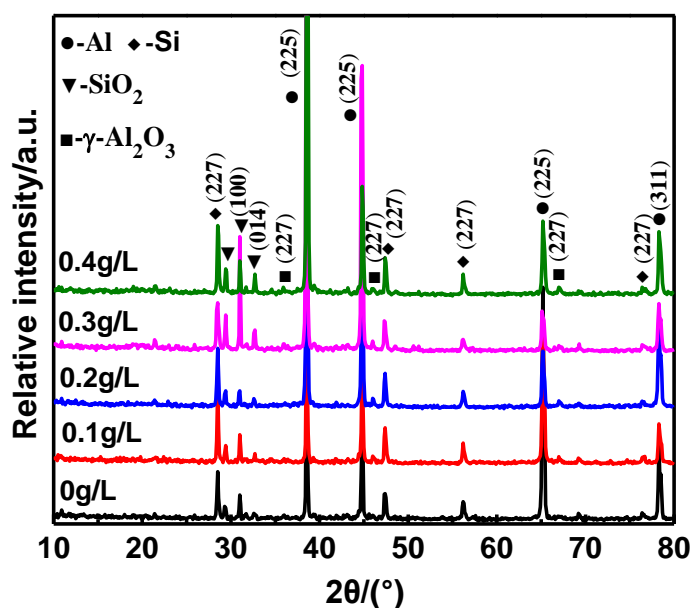
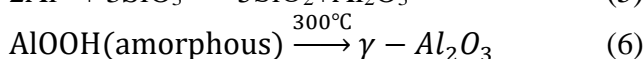
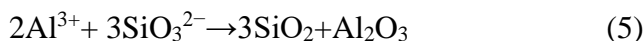
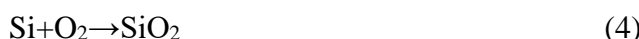


**Figure 4.** XRD results of the MAO coatings prepared using different  $\text{Nd}_2\text{O}_3$  particles concentrations.

### 3.4 The thickness and microhardness analysis

Microhardness and thickness tests were carried out on the specimens prepared using different  $\text{Nd}_2\text{O}_3$  particle concentrations, and the results are shown in Fig. 5. With the addition of the  $\text{Nd}_2\text{O}_3$  particles, the microhardness of the coatings increased, while the thickness of the coatings gradually increased and then decreased at the highest  $\text{Nd}_2\text{O}_3$  concentration of 0.4 g/L. The substrate hardness of ZL108 cast aluminum alloy is only 156.1 HV, while the hardness of the MAO coating prepared without  $\text{Nd}_2\text{O}_3$  particles is approximately 459.3 HV, approximately three times greater than that of the substrate. The hardness values of all the MAO coatings prepared with  $\text{Nd}_2\text{O}_3$  particles were much greater than those prepared without  $\text{Nd}_2\text{O}_3$  particles. The increment of hardness was ascribed to the

increase of oxidation voltage after adding  $\text{Nd}_2\text{O}_3$  particles, which led to the transition from amorphous  $\text{Al}_2\text{O}_3$  to crystalline  $\text{Al}_2\text{O}_3$ . In addition, the increase in the voltage increased the growth rate of the coatings; therefore, the thickness of the coatings increased with the addition of  $\text{Nd}_2\text{O}_3$  particles.

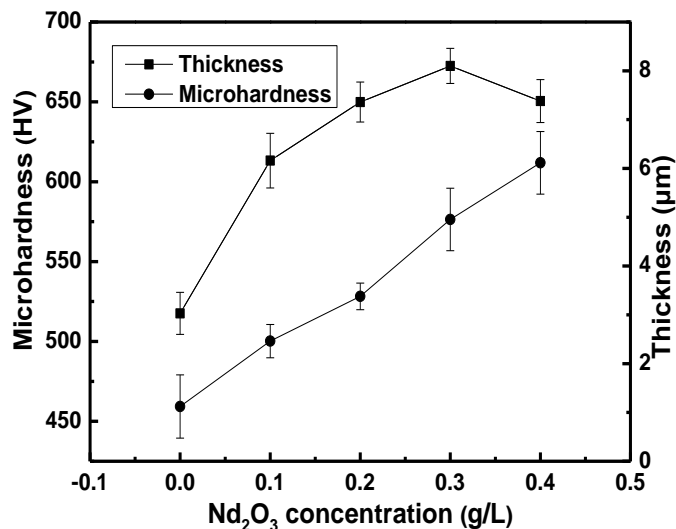


**Figure 5.** The microhardness and thickness of the MAO coatings prepared using different concentrations of  $\text{Nd}_2\text{O}_3$  particles.

### 3.5 The corrosion resistance of the coatings

The potentiodynamic polarization curves of ZL108 cast aluminum alloy samples in 3.5wt.% NaCl solution are shown in Fig. 6. Based on the approximately linear polarization behavior near the open-circuit potential (OCP), the polarization resistance ( $R_p$ ) values were determined from the Stern–Geary equation [16]:

$$R_p = \frac{b_a b_c}{2.303 i_{corr} (b_a + b_c)} \quad (7)$$

where  $b_a$  and  $b_c$  are the anodic/cathodic Tafel constants,  $i_{corr}$  is the corrosion current density, and  $E_{corr}$  is the corrosion potential.

Table 2 reports the results of the polarization curves analyzed by Tafel fitting. All the MAO-coated Al alloys showed a more positive  $E_{corr}$  and a much lower  $i_{corr}$  compared to the substrate Al alloy, which illustrates that the corrosion resistance was improved drastically through MAO treatment. With the addition of  $\text{Nd}_2\text{O}_3$  particles, the corrosion rate of the coatings slightly decreased, indicating that the corrosion resistance of the coatings was improved. On the one hand, the thickening of the coatings impeded the movement of eroding  $\text{Cl}^-$  ions to the substrate so that the corrosion rate of the coatings decreased. On the other hand, after adding the  $\text{Nd}_2\text{O}_3$  particles, the coatings became more compact and the number of micropores decreased, which were also beneficial to the improvement of the corrosion resistance of the coatings.

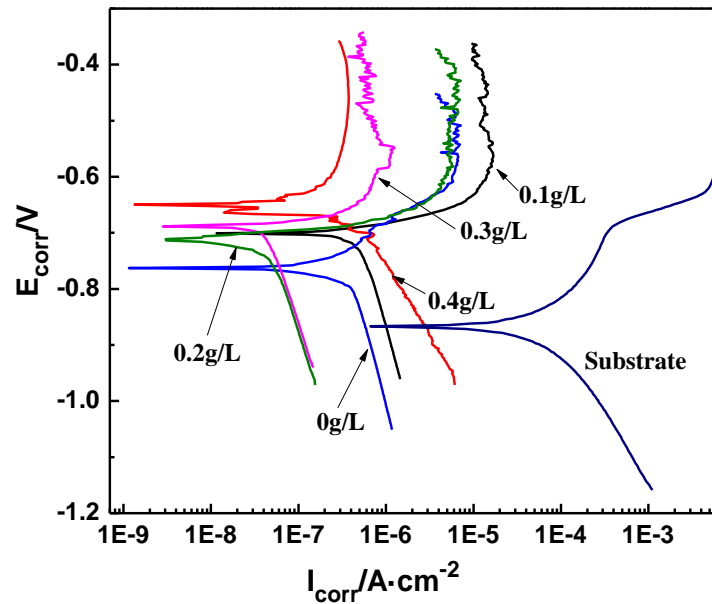


**Figure 6.** Polarization curves of the MAO coatings prepared using different concentration of  $\text{Nd}_2\text{O}_3$  particles (3.5% NaCl)

**Table 2.** Results of polarization curves analysis

Concentration (g/L)	$E_{\text{corr}}$ (V)	$I_{\text{corr}}$ (A/cm <sup>2</sup> )	Corrosion rate (mm/a)
Substrate	-0.87	$6.58 \times 10^{-5}$	0.72381
0	-0.70	$4.83 \times 10^{-7}$	$5.61 \times 10^{-3}$
0.1	-0.72	$4.58 \times 10^{-7}$	$4.72 \times 10^{-3}$
0.2	-0.75	$3.52 \times 10^{-7}$	$4.01 \times 10^{-3}$
0.3	-0.69	$4.09 \times 10^{-8}$	$5.75 \times 10^{-4}$
0.4	-0.68	$3.72 \times 10^{-8}$	$4.74 \times 10^{-4}$

### 3.6 The Crack resistance analysis

#### 3.6.1 The adhesive strength of the coatings

Scratch tests are usually used to evaluate the adhesion strength between the coating and the substrate, and results of the scratch tests are depicted in Fig. 6. It can be observed that the adhesion strength of the coatings increased gradually with the addition of  $\text{Nd}_2\text{O}_3$  particles, in accordance with the cross-sectional analysis, demonstrating that adding  $\text{Nd}_2\text{O}_3$  particles was beneficial to the improvement of adhesion strength between the coatings and the substrates, which reduced the risk of coating shedding. With an increase in the concentration of  $\text{Nd}_2\text{O}_3$  particles, the oxidation voltage increased comparatively, resulting that the substrate aluminum was directly transformed into crystalline alumina without large voids at the interface between the coatings and the substrate, and had better lattice matching [17]. In addition, the adhesive strength is related to the thickness and compactness of the coatings [18]. The coatings prepared with  $\text{Nd}_2\text{O}_3$  particles had higher thickness and

better compactness, thus the adhesive strength of the coatings was enhanced with the addition of  $\text{Nd}_2\text{O}_3$  particles.

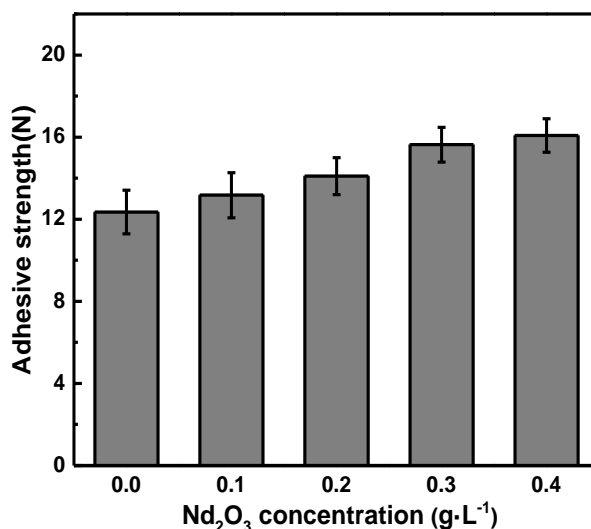


**Figure 7.** The adhesive strength of the MAO coatings prepared with different  $\text{Nd}_2\text{O}_3$  particle concentrations.

### 3.6.2 The thermal shock resistance of the coatings

The surface morphologies of coatings prepared using different  $\text{Nd}_2\text{O}_3$  particle concentrations after the thermal shock tests under different magnifications are shown in Fig. 8 and Fig. 9. The thermal shock resistance can directly reflect the anti-stripping capacity of the surface coatings with the alternative variation of temperature during the process [19]. In Fig. 8, it can be seen that no denting and peeling phenomenon occurred on the coating surface of the samples subjected to a temperature of  $500^\circ\text{C}$  for 50 cycles, which indicated that the coatings possessed a good thermal shock resistance. At the particle concentration of  $0\text{ g/L}$ , the surface of the coatings distributed many miniscule holes, while the number of holes decreased, and the coatings became denser with the addition of  $\text{Nd}_2\text{O}_3$  particles. At  $200\times$  magnification, it is obvious that cracks appeared on the surface of the coatings prepared without  $\text{Nd}_2\text{O}_3$  particles. Moreover, cracks on the coating surface decreased and even gradually vanished with an increase in the  $\text{Nd}_2\text{O}_3$  particle concentration, which demonstrated that adding  $\text{Nd}_2\text{O}_3$  particles in electrolytes could reduce cracks on the coatings and improve the thermal shock resistance of the coatings.

Zhang [20] had proposed the following formula for thermal shock resistance:

$$R = p\lambda/Ea \quad (8)$$

where  $R$  is the thermal shock resistance factor,  $p$  is the intensity,  $\lambda$  is the heat conductivity coefficient,  $E$  is the elasticity modulus, and  $a$  is the coefficient of thermal expansion of the coatings. The larger the  $R$  value is, the better is the thermal shock resistance. As mentioned above, with the addition of the  $\text{Nd}_2\text{O}_3$  particles, the compactness of the coatings was improved and the strength

increased accordingly [21]; therefore, the ability to resist thermal stress was enhanced, and the thermal shock resistance of the coatings increased. On the other hand, the thermal shock resistance of the coatings was also related to the interfacial adhesion strength between the coatings and the substrates. The increase in adhesion strength was beneficial to the improvement of the thermal shock resistance of the coatings.

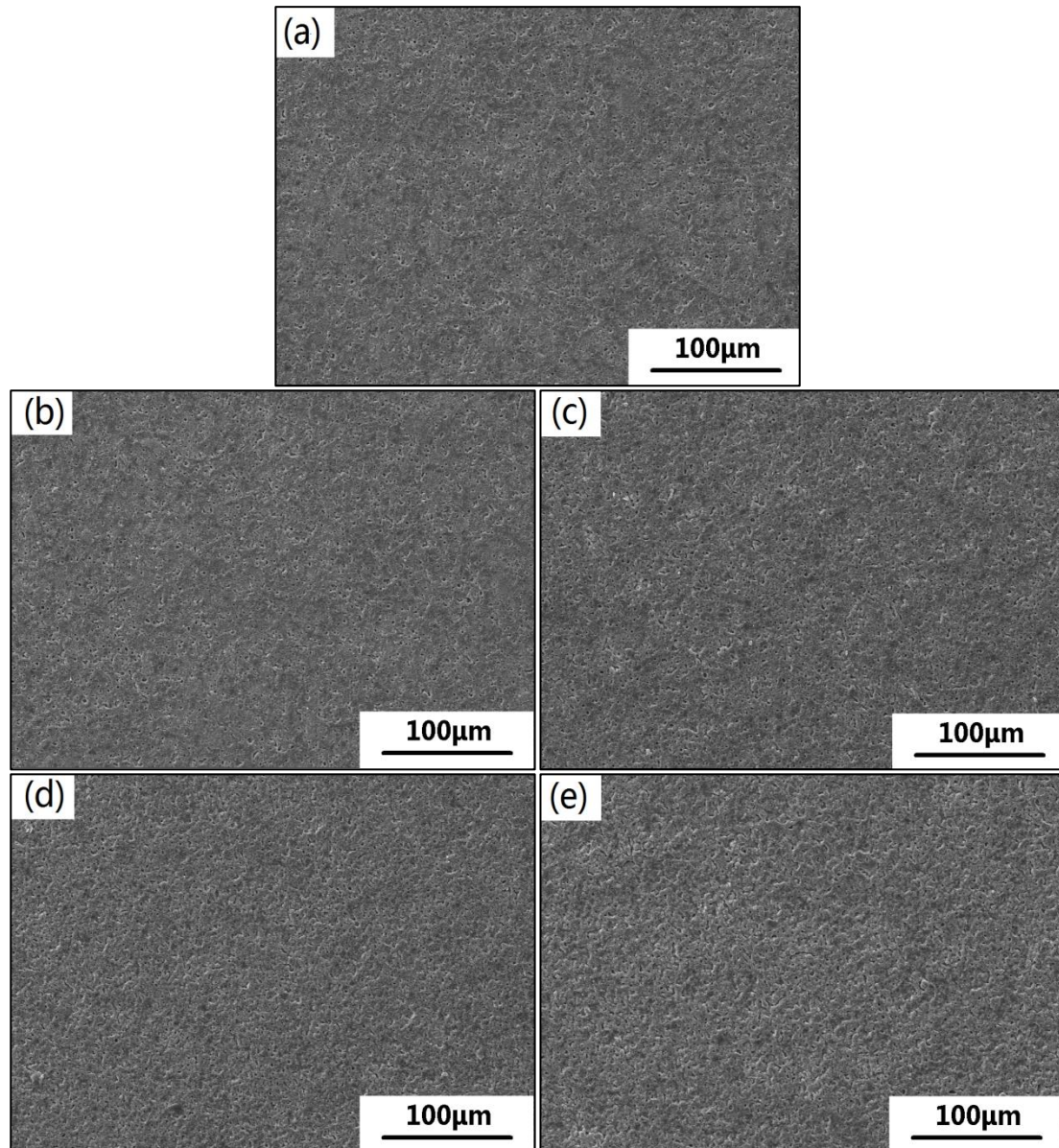


**Figure 8.** The morphology of the MAO coatings after thermal shock tests for 50 cycles at 200 times magnification:(a) 0 g/L, (b) 0.1 g/L, (c) 0.2 g/L, (d) 0.3 g/L, (e) 0.4 g/L.

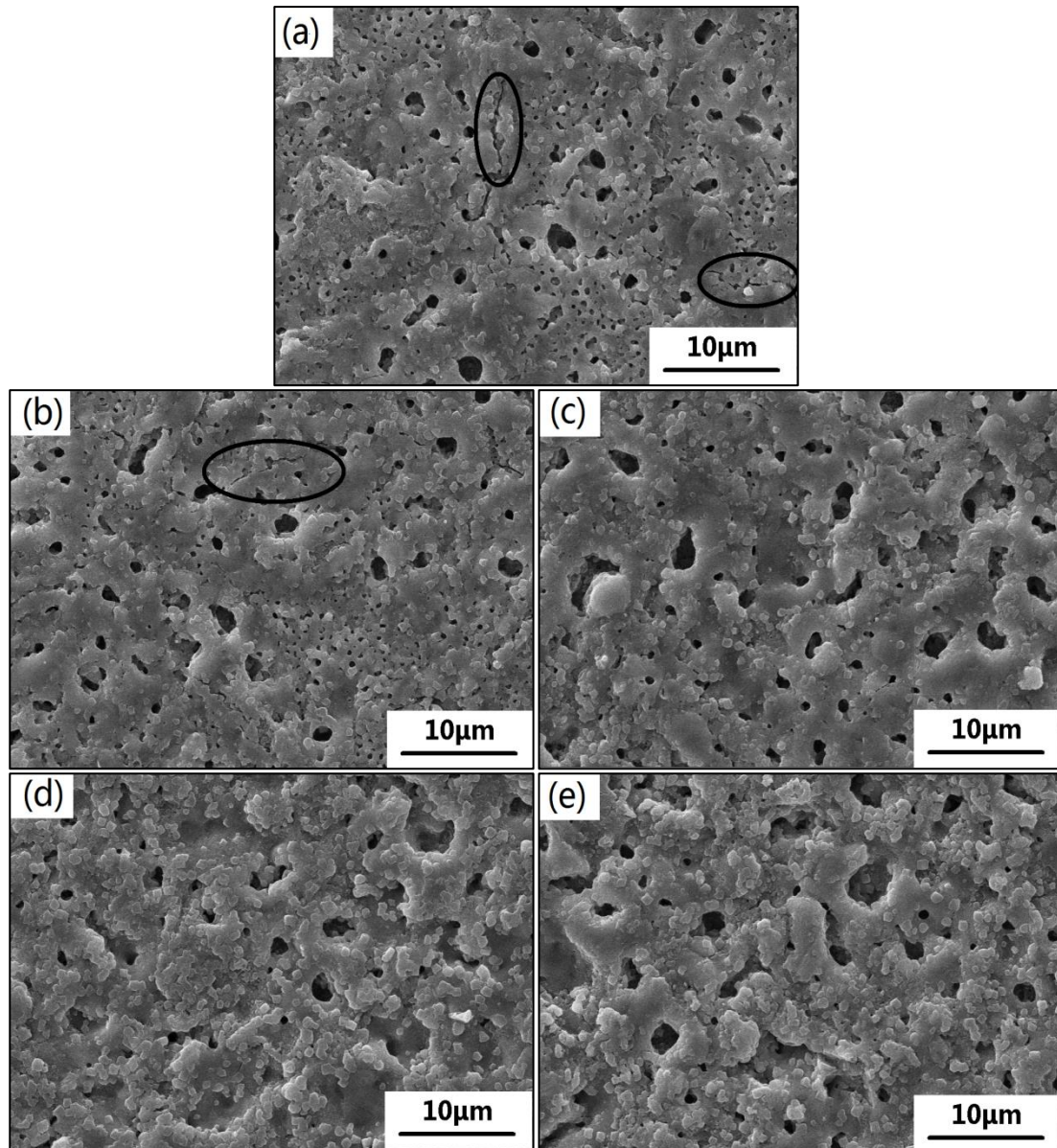


**Figure 9.** The morphology of the MAO coatings after thermal shock tests for 50 cycles at 2000 times magnification:(a) 0 g/L, (b) 0.1 g/L, (c) 0.2 g/L, (d) 0.3 g/L, (e) 0.4 g/L.

Adding  $\text{Nd}_2\text{O}_3$  particles raised the adhesion strength of the coatings, giving rise to the enhancement of the thermal shock resistance of the coatings. In short, the addition of  $\text{Nd}_2\text{O}_3$  particles can reduce the number of microcracks and decreased the possibility of coating peeling due to stress expansion, thereby improving the overall performance of the coatings.

#### 4. CONCLUSIONS

MAO coatings were fabricated on ZL108 cast aluminum alloy at different concentrations of  $\text{Nd}_2\text{O}_3$  particles. The addition of  $\text{Nd}_2\text{O}_3$  particles had apparent effects on the qualities of the coatings. With the addition of  $\text{Nd}_2\text{O}_3$  particles, the hardness of the coatings increased, and the thickness of the coatings initially increased and then decreased at a  $\text{Nd}_2\text{O}_3$  concentration of 0.4 g/L, in accordance with

the regularity of the voltage. Although the size of micropores increased with the addition of the Nd<sub>2</sub>O<sub>3</sub> particles, the number of micropores decreased and the coatings became more compact, as confirmed by the cross-sectional microstructures, thus the corrosion resistance was improved. The MAO coatings were mainly composed of  $\gamma$ -Al<sub>2</sub>O<sub>3</sub>, SiO<sub>2</sub> and Si, and the intensity patterns of  $\gamma$ -Al<sub>2</sub>O<sub>3</sub> and SiO<sub>2</sub> initially increased and then slowly decreased as the particle concentration increased. In addition, the thermal shock resistance was tremendously enhanced with the addition of Nd<sub>2</sub>O<sub>3</sub> particles, and the service life of the coatings was dramatically prolonged.

#### ACKNOWLEDGMENT

This work was supported by the Chunhui Project of Education Ministry of China (No. Z2011074); the Support Program of Wear and Friction Surface Engineering Research Center of Sichuan Provincial Education Department.

#### DECLARATION OF INTEREST

The authors declare that there are no conflicts of interest regarding the publication of this paper.

#### References

1. Z. J. Wang, L. N. Wu, W. Cai, A. Shan and Z. H. Jiang, *J. Alloys Compd.*, 505(2010)188.
2. Z. Shao, B. Kong, Y. Zhao and Z. Cai, *Surf. Eng.*, 30(2014)893.
3. C. C. Tseng, J. L. Lee, T. H. Kuo, S. N. Kuo, and K. H. Tseng, *Surf. Coat. Technol.*, 206(2012)3437.
4. Z. W. Li and S. C. Di, *J. Mater. Eng. Perform.*, 26(2017)1551.
5. C. J. Hu and M. H. Hsieh, *Surf. Coat. Technol.*, 258(2014)275.
6. P. Wang, T. Wu, H. Peng and X. Y. Guo, *Mater. Lett.*, 170(2016)171.
7. Y. N. Xue, X. Pang, B. L. Jiang and H. Jahed, *Int. J. Electrochem. Sci.*, 13(2018)7265.
8. M. Q. Tang, Z. Q. Feng, G. Li, Z. Z. Zhang and R. Z. Zhang, *Surf. Coat. Technol.*, 264(2015)105.
9. W. Yang, D. P. Xu, J. L. Wang, X. F. Yao and J. Chen, *Corros. Sci.*, 136(2018) 174.
10. P. Wang, J. Pu, J. H. Zhou, W. J. Cao, Y. T. Xiao, Z. Y. Gong and J. Hu, *Int. J. Electrochem. Sci.*, 13(2018)8995.
11. P. Wang, Y. T. Xiao, Z. H. Zhou, J. Pu, W. J. Cao, Z. Y. Gong and J. Hu, *Int. J. Electrochem. Sci.*, 14(2019)287.
12. H. X. Li, R. G. Song and Z. G. Ji, *Trans. Nonferrous. Met. Soc. China*, 23(2013)406.
13. C. R. Zhou, L. Y. Chai and X. Y. Liu, *J. Northeast. Univ.*, 31(2010)6.
14. J.M. Zhao, K.N. Ouyang, X. Xie and J.W. Zhang, *Int. J. Electrochem. Sci.*, 12(2017)2400.
15. S. Sarbishei, M. A. F. Sani, M. R. Mohammadi. *Ceram. Int.*, 42(2016) 8789.
16. H. P. Duan, C. W. Yan and F. H. Wang, *Electrochim. Acta*, 52(2007)3785.
17. Z.D. Liu, Z.Q. Xiang, Z.Y. Zhang, M.J. Sun and H. Fu, *Light Metal*, 1(2008)48.
18. P. Wang, T. Wu, Y.T. Xiao, J. Pu, X.Y. Guo, J. Huang and C.L. Xiang, *J. Mater. Eng. Perform.*, 25(2016) 3972.
19. Z. Ma, W. C. Qu and Z. C. Li. *Surf. Technol.*, 37(2008)52.
20. J. S. Zhang and Q. P. Wang, *J. Hebei Poly. Univ.*, 29(2007)91.
21. Z. W. Xue, F. Wu, Z. J. Li, X. W. Li, X. Luan and X. D. Luo, *J. Synthetic Cryst.*, 47(2018)1933.